



Shock-ignition effect in indirect-drive inertial confinement fusion approachS. Yu. Gus'kov  and G. A. Vergunova **Lebedev Physical Institute, Russian Academy of Sciences, Leninskii Prospect 53, Moscow 11991, Russia*

(Received 8 February 2024; accepted 29 May 2024; published 14 June 2024)

Shock-ignition effect in indirect-drive thermonuclear target is demonstrated on the base of numerical simulations. Thermonuclear gain (in relation to laser pulse energy) of a shock-ignited indirect-drive thermonuclear capsule is obtained, which is 22.5 times higher than that at a traditional spark ignition of the capsule with the same DT-fuel mass, wherein the shock-ignition laser pulse energy is 1.5 times less than the energy of a laser pulse at traditional spark ignition. To implement the shock-ignition effect in indirect-drive target, a rapid increase in radiation temperature is required over several hundred picoseconds at the final stage of thermonuclear capsule implosion. The ability of such a rapid response of radiation temperature to variation in the intensity of an x-ray-producing laser pulse is the main factor in the uncertainty of the degree of manifestation of the shock-ignition effect in an indirect-drive target. This circumstance, first of all, requires experimental study.

DOI: [10.1103/PhysRevE.109.065209](https://doi.org/10.1103/PhysRevE.109.065209)**I. INTRODUCTION**

The shock-ignition method [1,2] is capable to significantly increase the energy efficiency in direct-drive inertial confinement fusion (ICF). A distinctive feature of the method is to provide a stronger separation of the processes of implosion and stagnation of a thermonuclear capsule compared to the traditional approach to spark ignition [3,4]. The latter is designed for use in a single-step profiled laser pulse. The shock ignition involves the use of a two-step pulse with a high power spike at the end of the pulse, which is intended to generate an ignition shock wave. The shock-ignition physics in relation to the direct drive is being actively investigated. The first step of shock-ignition pulse has the same behavior of temporary power profiling as in the case of traditional direct-drive ignition (see, for example, [5–7]). A submegajoule shock-ignition pulse of third-harmonic Nd laser pulse intended to ignite the target with, approximately, 1 mg DT-mass and 0.1 cm radius should include the first step with gradually increased power within a few nanoseconds from several TW to the value of several tens of TW, which retains for the next several nanoseconds. This part of the pulse, as in the case of the traditional approach, is intended for slow low-entropy compression of the target. The spike power increases very quickly (in a few hundred picoseconds) to a value of 400–600 TW, which maintains within the next few hundred picoseconds [1,2]. The spike should provide the generation of a powerful ignition shock wave with pressure of about 100–200 Mbar [8–11]. The central ignition region (hot spot) is formed at a high energy concentration as a result of the collision of one or more diverging and converging shock waves.

To date, a large amount of knowledge has been accumulated relating to the physics of shock ignition in the direct drive scheme. Thus, the results of theoretical studies related

to ignition shock wave generation, hot spot formation, hydrodynamic stability of implosion, role of laser-accelerated fast electrons, and thermonuclear gain of shock-ignited target can be found in [1,2,8–19]. In the experiments [20–30], several aspects of shock ignition are investigated, such as ablation pressure formation and fast electron generation driven by laser pulse with spike intensity. This situation is due to the current lack of a laser installation capable to provide ignition of a thermonuclear target under direct spherically symmetric irradiation with laser beams.

The only installation capable of igniting a thermonuclear target is the NIF (LLNL, USA) [31] with the third-harmonic Nd laser pulse energy of about 2 MJ. However, this installation is primarily intended for the indirect-drive thermonuclear capsule [32,33] located inside a hohlraum in which the initial laser pulse is converted into a soft x-ray flux. The laser beam focusing scheme is designed to use a cylindrical or quasicylindrical hohlraum with two-way input of laser beams inside through the end entrance holes. This focusing scheme is not intended to provide spherically symmetric irradiation of a thermonuclear capsule with laser beams in order to conduct experiments not only with indirect, but also with direct irradiation.

In the experiments with indirect-drive targets on the NIF facility, the appreciable results were achieved during the last three years using the conventional spark ignition method. In 2021, the results of experiments were published [34,35], in which the neutron yield of $N = 4.8 \cdot 10^{17}$ was recorded at the laser pulse energy of about 1.9 MJ. The released energy of DT reactions (fusion yield) is 1.37 MJ, which corresponds to thermonuclear gain in relation to laser energy, i.e., the ratio of the fusion yield to the input laser energy, $G_L = 0.72$. According to the data [36], the target ignition with a G_L of about 1.9 was achieved. On July 29, 2023 the fusion yield was about 3.88 MJ. The neutron yield was about $1.4 \cdot 10^{18}$.

The efficiency of applying the shock ignition to the indirect drive target is a reasonable question. Especially so,

*Contact author: vergunovaga@lebedev.ru

TABLE I. Several experimental and numerical data relating to shot N140520.

	Experimental data [38,39]	LLNL simulation [40]	
		N140520	1D
Laser energy (MJ)	1.764	1.76	1.76
Peak radiation temperature T_R (eV)	322	306	
Fuel velocity (km/s)	367–387	375–397	
Total DT neutron yield	$8.98 \cdot 10^{15}$	$1.1 \cdot 10^{17}$	$2.1 \cdot 10^{16}$
Neutron yield (kJ)	25.3	310	59.2
Gain of the target N140520 with respect to laser pulse energy G_L	0.014	0.18	0.034

because the calculations of [37] show that using the technical characteristics of a NIF laser, it is possible to generate a laser-induced x-ray pulse with peak power at the final stage acceptable for the application of shock ignition.

In this paper, the effect of shock ignition is demonstrated on the base of end-to-end simulations of the radiation hydrodynamics of the indirect drive target for the NIF conditions. The second section contains the problem statement with justification of the target and simulation method selections. The results of numerical simulation of shock-ignited indirect-drive targets are presented in the third section.

II. PROBLEM STATEMENT

Shock-ignition effect is demonstrated for one of the targets proposed at LLNL in 2014–2018 for experimental and computational studies of the traditional spark ignition of an indirect-drive target. To mark this target and the laser pulse intended for it, the experiment number N140520 is used, according to the data of [38–40]. The choice of this experiment was supported by the fact that the target and laser pulse parameters had been described in sufficient detail in [38–40]. The “research” target N140520 did not provide ignition. This fact further stimulated applying a shock ignition to this target. There are several data relating to the N140520 shot experiment, as well as to one-dimensional (1D) and two-dimensional (2D) simulations of this shot presented, according to [38–40], in the third and fourth columns of Table I. According to the one-dimensional LLNL calculations, gain of the target N140520 with respect to laser pulse energy was only $G_L \approx 0.18$ (Table I). In experiments of those years with laser pulse energy of about 1.7 MJ, the gain was $G_L \approx 0.014$, which was 13 times smaller than the result of a 1D simulation. One of the main reasons, in particular, was insufficient degree of the minimization of a negative impact of hydrodynamic instabilities on thermonuclear capsule implosion [41,42].

Below, parameters of the target and the laser pulse N140520 are presented, according to the data of [38–40]. The target N140520 is a cylinder hohlraum of 9.43 mm length and 5.75 mm diameter, in the geometric center of which a thermonuclear capsule is placed. The walls of the 30 μm thick hohlraum are made of Au. A depleted uranium 7 μm thick

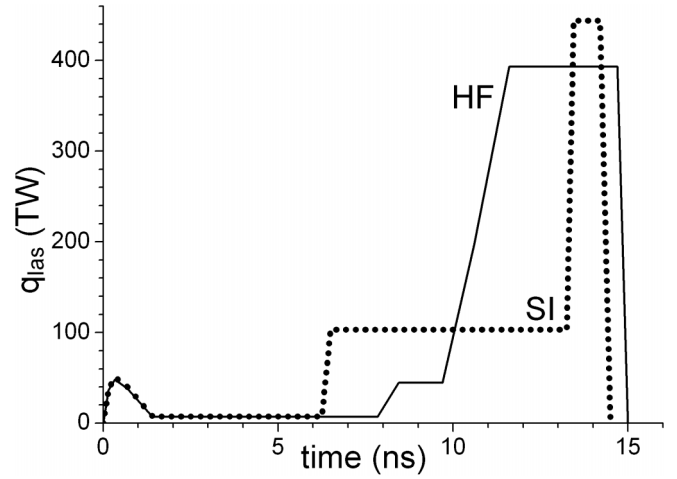


FIG. 1. The laser pulse used to irradiate the target in experiment N140520 [36,37] is shown by a solid curve. The laser pulse for irradiating a target with the same DT-fuel mass of thermonuclear capsule at shock ignition is shown by a dotted curve.

layer is encapsulated from the inside of the wall at a depth of 0.7 μm . The two laser entrance holes of 3.1 mm diameter are positioned at the hohlraum ends. The thermonuclear capsule is a spherical shell with an outer surface diameter of 2.25 mm. The outer layer of the capsule is the plastic ablator with a thickness of 178 μm . The ablator of the capsule N140520 had the layer doped by Si up to 2% by weight with a thickness of 51.6 μm , located on the side of the DT ice. The thickness of the internal layer of DT ice frozen onto the inner ablator surface is 69 μm . The density of the residual DT gas is 0.3 mg/cm³. The laser pulse N140520 with an energy of 1.76 MJ and a duration of 15 ns belonged to the “high foot” (HF) type. In the last high-intensity part of the pulse with a duration of 3 ns, the power was 393 TW. The dependence of pulse power on time is shown in Fig. 1.

Numerical simulation of this work was performed using the 1D radiative hydrodynamic code RADIANT [43–46]. In this code, the two-temperature hydrodynamic equations are solved together with a radiation transfer equation in the multigroup spectral approximation. Spectral optical constants are calculated according to the THERMOS database [47,48]. The real equation of state take into account the kinetics of ionization and cold pressure, as well as plasma heating by DT-reaction α particles. The laser light is absorbed by the bremsstrahlung mechanism.

In the experiment, laser energy is converted to thermal x-ray radiation at the inner surface of cylindrical hohlraum. 1D RADIANT code simulations are performed for laser pulse interaction with the inner surface of a spherical converter. At the same time, input laser energy distribution inside a spherical converter is determined by a comparison of the energy balance equations in cylindrical and spherical geometries [44]. Iterations were made to improve the fit of 1D-model simulation data to experimental ones. Varied in these iterations was the laser energy incident on the inner wall of the spherical hohlraum in order to reach a better match between the radiation temperature T_{rad} in the hohlraum cavity and the experimental data or the simulation data obtained at the LLNL

and published in [38–40]. By such a way it is established that the equivalent spherical converter radius is equal to 3750 μm . Eventually, the RADIANT code simulation results are in good agreement with the data of numerical modeling and experiments published in [38–40]. The peak radiation temperature of x-ray pulse of 322 eV, the maximum velocity of capsule implosion of 364 km/s, the implosion time of 15.88 ns, the time-width of thermonuclear burn (at half-height of the fusion energy release rate) of 142 ps, the DT-neutron and fusion yields, respectively, of $1.7 \cdot 10^{17}$ and 0.48 MJ, as well as the gain G_L of 0.27 were obtained in the RADIANT code simulation with target and laser pulse N140520. In the 1D simulations LLNL accompanying the experiment [38–40], the maximum value of the radiation temperature was 306 eV, the maximum velocity was 397 km/s, the implosion time was 15.97 ns, the DT neutron yield, the fusion yield, and the gain were, respectively, $1.1 \cdot 10^{17}$, 0.31 MJ, and $G_L \approx 0.18$. In the experiments [38–40] neutron yield of $9 \cdot 10^{15}$, maximum radiation temperature—about 322 eV, maximum implosion velocity—367–387 km/s, implosion time—15.91 ns, and duration of target burning—111 ps were obtained. Such a favorable result of comparison of RADIANT code data and those of [38–40] for traditional indirect-drive spark ignition became the argument to use RADIANT code for modeling the indirect-drive shock ignition.

III. SHOCK IGNITION OF INDIRECT-DRIVE TARGET

The main requirement for modifying the target and the laser pulse N140520 to demonstrate the shock-ignition effect is maintenance of spike power at the level of about 400 TW close to the maximum value of laser pulse N140520 shown in Fig. 1. Such a condition allows assuming that the shock-ignition pulse corresponds to the technical capabilities of the NIF installation. Based on a series of optimization calculations, target and laser pulse parameters were determined when a strong shock ignition effect is appeared. Next, the abbreviation SI will be used for the target and the laser pulse at shock ignition. The time dependence of SI-pulse power is shown in Fig. 1. Up to 6.25 ns, the pulse coincides with the pulse N140520. Further, the power of the SI-pulse is kept 100 TW for about 6.75 ns. Then, during 0.2 ns, the power increases to a maximum spike power of 450 TW, which is maintained for the next 0.75 ns until the end of the pulse. The total duration of the SI pulse is 14.5 ns, which is 0.5 ns less than the pulse N140520. The main difference between the SI pulse for indirect drive and the SI pulse for direct drive consists in spike parameters. In the case of indirect drive, the spike power is approximately 1.5 times less, and the spike duration is 1.5 times longer as compared to those for the case of direct drive. The increased duration is due to the delay in the x-ray pulse formation relative to the laser pulse, which is determined, in particular, by the heat capacity of the hohlraum wall [32,37].

The SI target differs from the target N140520 by thickness (mass) of thermonuclear capsule ablator only. With the same mass and inner surface radius of the DT layer, the ablator mass is reduced by about 1.5 times as compared to the thermonuclear capsule of the target N140520. As a result, the thickness of the shock-ignition target ablator was 118.5 μm . The ablator

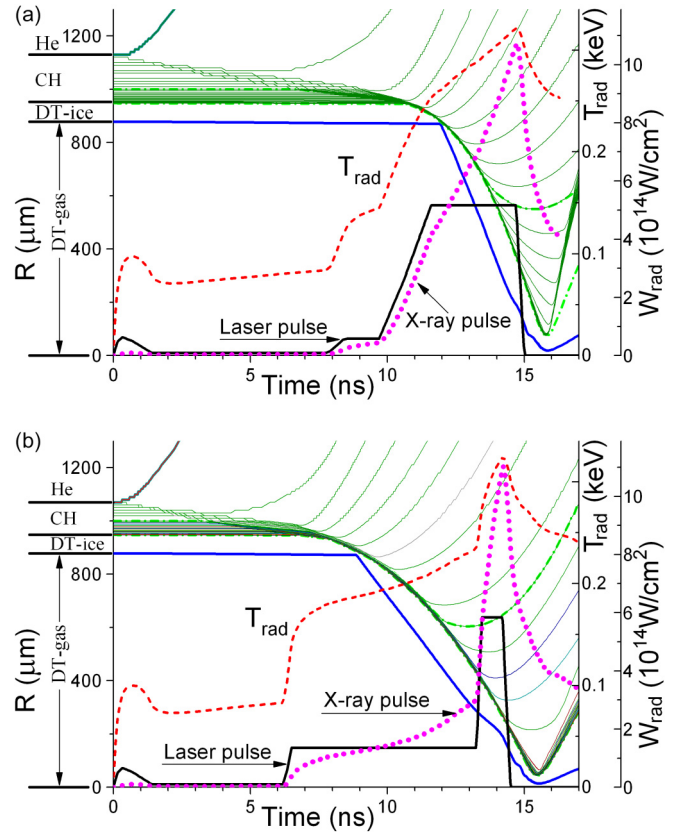


FIG. 2. Temporal dependence of the internal radii of thermonuclear capsule ($R-t$ diagram of capsule implosion), radiation temperature in hohlraum (T_{rad} , dashed curves) and energy flux density of x-ray pulse (W_{rad} , dotted curves) heating the capsule as calculated by the RADIANT code of the N140520 target (a) and the SI target (b) having the same mass of DT fuel. To the left of the R axis, the initial positions of DT-ice and CH-ablator layers are shown. $R-t$ dependence of boundary between DT ice and ablator is shown by the blue solid curve. The laser pulse is shown schematically by the black solid curve.

thickness decrease corresponds to the decrease of ablation rate according to its dependence on laser intensity $I^{9/40}$ [32] when the power of compressive part of the SI pulse (100 TW) is four times less compared to pulse N140520 power (393 TW). The total energy of the SI pulse is 1.2 MJ, which is approximately 1.4 times less compared to pulse N140520 (1.76 MJ). The capsule with ablator thickness of 118.5 μm used in our numerical simulation of the SI target had the same layer doped by Si up to 2 wt.% of 51.6 μm thickness as the capsule of the N140520 target.

In 1D RADIANT simulation with the above described SI target and SI pulse demonstrates the gain $G_L = 6.1$, which is approximately 22 times higher than the 1D gain at the traditional spark ignition with the target N140520.

Figure 2 shows the time dependence of the internal radii of thermonuclear capsule ($R-t$ diagram of capsule implosion), the radiation temperature in hohlraum (T_{rad}), and the energy flux density of x-ray pulse (W_{rad}) heating the capsule as calculated by the RADIANT code of the N140520 target [Fig. 2(a)] and the SI [Fig. 2(b)] target. HF and SI laser pulses described above also are schematically shown on these figures.

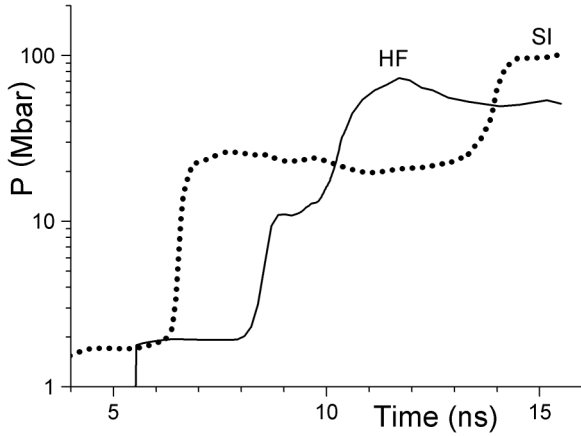


FIG. 3. The time dependences of ablation pressure for the SI target (the dashed curve) and target N140520 (the solid curve).

The time dependences of radiation temperature T_{rad} and x-ray energy flux density W_{rad} follow to the time dependence of laser pulse. For the SI pulse during the period of spike power growth from 13.25 ns to 13.45 ns, the values T_{rad} and W_{rad} monotonically increase from 212 eV and $3 \cdot 10^{14}$ W/cm² up to 274 eV and $5.6 \cdot 10^{14}$ W/cm². During the period of constant spike power from 13.45 ns to 14.2 ns, these values continue to grow to the maximum values of 324 eV and $1.1 \cdot 10^{15}$ W/cm².

The maximum radiation temperature is, practically, the same as when the target N140520 is ignited using the traditional spark ignition approach (322 eV, as it was mentioned in the previous section). The time delay of x-ray pulse maximum formation with respect to the time when the spike reaches the maximum power is about 0.75 ns. As already mentioned, it is caused, in particular, by the heat capacity of the hohlraum wall. Despite this, the increase in the x-ray energy flux density during a spike action turns out to be steep enough to generate an igniting shock wave.

Figure 3 shows the time dependences of the ablation pressure for the SI target and target N140520. The pressure actually changes with the laser pulse power (Fig. 1). The maximum ablative pressure (100 Mbar) in the SI target is 1.4 times larger than in the target N140520 (70 Mbar). Thus, the calculation results indicate the manifestation of a strong shock-ignition effect at the approximate conservation of spike power at a level of maximum power of laser pulse N140520 used in NIF experiments.

To demonstrate the SI effect, the numerical simulations in this work were performed for the SI target with minimal changes made compared to a specific indirect-drive spark-ignition target. An important direction for further research is the comprehensive optimization of both the parameters of the SI target and the laser pulse. In particular, the important issue is the sensitivity of the SI effect in an indirect-drive target to spike parameters through the response of radiation temperature to a rapid increase in spike intensity.

In the simulations presented in this paper, over the entire duration of the spike, 0.95 ns (0.2 ns of which is the duration of spike-intensity rise and 0.75 ns is the duration of the constant maximum intensity), the time-average rate of

increase in radiation temperature is 118 eV/ns. The rate of increase in radiation temperature exceeds the above average value at the stage of increasing spike intensity (at a relatively small radiation temperature) and is significantly lower than this value while maintaining the maximum spike intensity (at a high radiation temperature). In this case, the average rate of growth of the relative radiation temperature (normalized to its value at the beginning of the increase) is about 0.58 ns^{-1} .

As compared to similar calculations of the radiation temperature evolution, it is possible to use the results of paper [37]. In that paper, during the spike with approximately the same duration of 1 ns, of which 0.2 ns is the duration of the spike-intensity rise and 0.75 ns the duration of the constant maximum intensity, the average rate of radiation temperature growth is 140 eV/ns with the average growth of the relative temperature (normalized to its value at the beginning of the rise) of about 0.8 ns^{-1} .

In experiments at the NIF facility, the shortest rise time of the laser pulse intensity is about 1 ns [49]. In experiments on spark ignition with a HF laser pulse [50], the rate of radiation temperature growth in a sufficiently heated hohlraum at the stage of rapid increase in laser pulse intensity over the period of 8–9 ns was about 60 eV/ns. Simulations using the RADIANT code under the conditions of the above experiment at the same stage of laser pulse growth gives a similar radiation temperature rise rate of about 80 eV/ns [44]. At the same time, the rate of increase in relative radiation temperature (normalized to its value at the beginning of the increase) in the experiment is about 0.6 ns^{-1} [50], which is a value close to the average rate of increase in relative radiation temperature in the calculations of the SI ignition target using the RADIANT code (0.58 ns^{-1}). The rapid increase in radiation temperature over several hundred picoseconds at the final stage of thermonuclear capsule implosion is the main factor in the uncertainty of the degree of manifestation of the shock-ignition effect in an indirect-drive target. The ability of such a rapid response of radiation temperature to variation in the intensity of x-ray-producing laser pulse, first of all, requires experimental study.

A comparative presentation of RADIANT code results for the SI target and target N140520 is presented in Table II.

Shock ignition leads to a hot spot with significantly higher values of maximum ion temperature of 15 keV and areal density of $0.32 \text{ g} \cdot \text{cm}^{-2}$ compared to traditional spark ignition approach, when these values are 5 keV and $0.11 \text{ g} \cdot \text{cm}^{-2}$ only. Moreover, for thermonuclear capsules of the SI target, this is achieved at the SI laser pulse energy 1.5 times less than the energy of laser pulse N140520 despite the SI capsule and target N140520 having equal DT-fuel masses. As a result, the shock ignition provides efficient burning of a compressed thermonuclear capsule with thermonuclear gain of 6.1 and DT-fuel burnout of 12.6%, whereas these values for the target and laser pulse N140520 are, respectively, 0.27 and 0.88% only.

IV. CONCLUSIONS

A simulation and theoretical demonstration of a possibility to effectively use shock-ignition approach to indirect-drive thermonuclear capsule with a pulse of laser-induced x-ray pulse is presented. The numerical simulations

TABLE II. Several results of RADIAN-code simulations for the SI target and target N140520.

	SI target	Target N140520
Laser pulse energy (MJ)	1.2	1.76
Laser pulse duration (ns)	14.5	15
Released energy of fusion reactions (MJ)	7.34	0.480
Maximum radiation temperature in hohlraum (eV)	324	322
Time of thermonuclear target implosion (ns)	15.55	15.88
Neutron yield	$2.6 \cdot 10^{18}$	$1.4 \cdot 10^{17}$
Thermonuclear gain relative to laser energy	6.1	0.27
DT-fuel burnout in fusion reactions (%)	12.6%	0.88%
Areal density of DT fuel at the moment of maximum compression of the capsule ($\text{g} \cdot \text{cm}^{-2}$)	0.88	0.39
Areal density of DT-fuel hot spot with average temperature exceeding 4.5 keV at the time of maximum compression of the capsule ($\text{g} \cdot \text{cm}^{-2}$)	0.32	0.11
The maximum ion temperature in DT fuel at the time of maximum compression of the capsule (keV)	16	5
The maximum ion temperature in DT fuel during the thermonuclear burning (keV)	48	15

of indirect-drive targets with thermonuclear capsules of the equal DT-fuel masses justify that shock-ignition provided the thermonuclear gain 20 times greater, and at the laser

pulse energy 1.5 times lower as compared to traditional spark ignition.

An important circumstance is the fact that shock ignition of indirect-drive target can be carried out while maintaining the spike power at the level of the maximum power of laser pulse (400 TW) as used in the traditional spark ignition scheme.

In this work, the SI effect is demonstrated based on 1D simulations. An important direction for further theoretical research in this area is to study the degree of hydrodynamic stability of the SI scheme based on 2D and 3D simulations. Another important issue is to study the robustness of the SI indirect-drive scheme versus laser pulse timing and establish SI laser pulse timing windows, as it is a study in direct-drive SI approach. The ability of rapid increase in radiation temperature over several hundred picoseconds at the final stage of thermonuclear capsule implosion is the main factor in the uncertainty of the degree of manifestation of the shock-ignition effect in an indirect-drive target. This circumstance requires experimental study.

The demonstrated potential of increasing the energy efficiency of indirect drive target due to the use of shock ignition indicates the relevance of further research in order to conduct the experiments in this area.

ACKNOWLEDGMENTS

The authors are grateful to R.A. Yakhin for useful discussions and to I. Ya. Doskoch for the help in the preparation of the manuscript.

- [1] V. A. Shcherbakov, *Sov. J. Plasma Phys.* **9**, 240 (1983).
- [2] R. Betti, C. D. Zhou, K. S. Anderson, J. L. Perkins, W. Theobald, and A. A. Solodov, *Phys. Rev. Lett.* **98**, 155001 (2007).
- [3] V. B. Rozanov, C. P. Verdon, M. Decroisette *et al.*, *Energy from Inertial Fusion* (IAEA, Vienna, 1995).
- [4] S. Atzeni and J. Meyer-Ter-Vehn, *The Physics of Inertial Fusion* (Oxford University Press, New York, 2004), p. 47.
- [5] R. S. Craxton, K. S. Anderson, T. R. Boehly *et al.*, *Phys. Plasmas* **22**, 110501 (2015).
- [6] V. Brandon, B. Canaud, M. Temporal, and R. Ramis, *Nucl. Fusion* **54**, 083016 (2014).
- [7] S. A. Bel'kov, S. V. Bondarenko, G. A. Vergunova *et al.*, *J. Exp. Theor. Phys.* **121**, 686 (2015).
- [8] X. Ribeyre, M. Lafon, G. Schurtz *et al.*, *Plasma Phys. Control. Fusion* **51**, 124030 (2009).
- [9] S. Atzeni, A. Marocchino, A. Schiavi, and G. Schurtz, *New J. Phys.* **15**, 045004 (2013).
- [10] M. Lafon, X. Ribeyre, and G. Schurtz, *Phys. Plasmas* **20**, 022708 (2013).
- [11] S. Atzeni, X. Ribeyre, G. Schurtz *et al.*, *Nucl. Fusion* **54**, 054008 (2014).
- [12] S. A. Bel'kov, S. V. Bondarenko, S. G. Garanin *et al.*, *J. Exp. Theor. Phys.* **131**, 636 (2020).
- [13] K. S. Anderson, R. Betti, P. W. McKenty *et al.*, *Phys. Plasmas* **20**, 056312 (2013).
- [14] S. Atzeni, A. Marocchino, and A. Schiavi, *Phys. Plasmas* **19**, 090702 (2012).
- [15] A. J. Schmitt, J. W. Bates, S. P. Obenshain *et al.*, *Phys. Plasmas* **17**, 042701 (2010).
- [16] S. Atzeni, A. Schiavi, A. Marocchino *et al.*, *Plasma Phys. Control. Fusion* **53**, 035010 (2011).
- [17] S. Yu. Gus'kov, N. N. Demchenko, N. V. Zmitrenko *et al.*, *J. Exp. Theor. Phys.* **130**, 748 (2020).
- [18] W. L. Shang, R. Betti, S. X. Hu, K. Woo, L. Hao, C. Ren, A. R. Christopherson, A. Bose, and W. Theobald, *Phys. Rev. Lett.* **119**, 195001 (2017).
- [19] S. Yu. Gus'kov, N. N. Demchenko, E. O. Dmitriev *et al.*, *Plasma Phys. Control. Fusion* **64**, 045011 (2022).
- [20] D. Batani, L. Antonelli, F. Barbato *et al.*, *Nucl. Fusion* **59**, 032012 (2019).
- [21] R. H. H. Scott, K. Glize, L. Antonelli, M. Khan, W. Theobald, M. Wei, R. Betti, C. Stoeckl, A. G. Seaton, T. D. Arber, D. Barlow, T. Goffrey, K. Bennett, W. Garbett, S. Atzeni, A. Casner, D. Batani, C. Li, and N. Woolsey, *Phys. Rev. Lett.* **127**, 065001 (2021).
- [22] W. Theobald, A. Bose, R. Yan *et al.*, *Phys. Plasmas* **24**, 120702 (2017).
- [23] A. Tentori, A. Colaitis, W. Theobald *et al.*, *Phys. Plasmas* **28**, 103302 (2021).
- [24] W. Theobald, R. Nora, M. Lafon *et al.*, *Phys. Plasmas* **19**, 102706 (2012).

- [25] S. Zhang, C. M. Krauland, J. Peebles *et al.*, *Phys. Plasmas* **27**, 023111 (2020).
- [26] D. Batani, L. Antonelli, S. Atzeni *et al.*, *Phys. Plasmas* **21**, 032710 (2014).
- [27] J. Trela, W. Theobald, K. S. Anderson *et al.*, *Phys. Plasmas* **25**, 052707 (2018).
- [28] G. Cristoforetti, A. Colaitis, L. Antonelli *et al.*, *Europhys. Lett.* **117**, 35001 (2017).
- [29] M. Hohenberger, W. Theobald, S. X. Hu *et al.*, *Phys. Plasmas* **21**, 022702 (2014).
- [30] S. Baton, A. Colaitis, C. Rousseaux *et al.*, *High Energy Density Phys.* **36**, 100796 (2020).
- [31] E. Moses and C. R. Wuest, *Fusion Sci. Technol.* **47**, 314 (2005).
- [32] J. D. Lindl, *Phys. Plasmas* **2**, 3933 (1995).
- [33] S. W. Haan, J. D. Lindl, D. A. Callahan *et al.*, *Phys. Plasmas* **18**, 051001 (2011).
- [34] H. Abu-Shawareb, R. Acree, P. Adams *et al.*, *Phys. Rev. Lett.* **129**, 075001 (2022).
- [35] H. Abu-Shawareb, R. Acree, P. Adams *et al.*, *Phys. Rev. Lett.* **132**, 065102 (2024).
- [36] A. L. Kritcher, A. B. Zylstra, C. R. Weber *et al.*, *Phys. Rev. E* **109**, 025204 (2024).
- [37] W. Trickey and J. Pasley, *Plasma Phys. Control. Fusion* **61**, 105010 (2019).
- [38] T. Döppner, D. A. Callahan, O. A. Hurricane *et al.*, *Phys. Rev. Lett.* **115**, 055001 (2015).
- [39] S. W. Haan, A. L. Kritcher, D. S. Clark, S. A. Yi, A. B. Zylstra, J. E. Ralph, and C. R. Weber, Report LLNL-TR-741418 (2017).
- [40] A. L. Kritcher, D. Clark, S. Haan *et al.*, *Phys. Plasmas* **25**, 056309 (2018).
- [41] O. A. Hurricane, D. A. Callahan, D. T. Casey *et al.*, *Nature (London)* **506**, 343 (2014).
- [42] A. B. Zylstra, A. L. Kritcher, O. A. Hurricane *et al.*, *Phys. Rev. E* **106**, 025202 (2022).
- [43] G. A. Vergunova and V. B. Rozanov, *Laser Part. Beams* **17**, 579 (1999).
- [44] V. B. Rozanov and G. A. Vergunova, *J. Exp. Theor. Phys.* **121**, 747 (2015).
- [45] V. B. Rozanov and G. A. Vergunova, *J. Exp. Theor. Phys.* **124**, 182 (2017).
- [46] V. B. Rozanov and G. A. Vergunova, *J. Exp. Theor. Phys.* **127**, 786 (2018).
- [47] A. F. Nikiforov, V. G. Novikov, and V. B. Uvarov, *Quantum-Statistical Models of Hot Dense Matter: Methods for Computation Opacity and Equation of State* (Birkhauser, Basel, 2005).
- [48] D. A. Kim, I. Yu. Vichev, A. D. Solomyannaya, and A. S. Grushin, KIAM Preprint No. 58 (Keldysh Inst. Appl. Math., Moscow, 2020).
- [49] H. S. Park, O. A. Hurricane, D. A. Callahan, D. T. Casey, E. L. Dewald, T. R. Dittrich, T. Doppner, D. E. Hinkel, L. F. BerzakHopkins, S. LePape, T. Ma, P. K. Patel, B. A. Remington, H. F. Robey, J. D. Salmonson, and J. L. Kline, *Phys. Rev. Lett.* **112**, 055001 (2014).
- [50] T. R. Dittrich, O. A. Hurricane, D. A. Callahan, E. L. Dewald, T. Doppner, D. E. Hinkel, L. F. BerzakHopkins, S. LePape, T. Ma, J. L. Milovich, J. C. Moreno, P. K. Patel, H. S. Park, B. A. Remington, J. D. Salmonson, and J. L. Kline, *Phys. Rev. Lett.* **112**, 055002 (2014).